Half-life measurement of the 199-keV isomeric state in math xmlns="http://www.w3.org/1998/Math/MathML">mmultiscripts>mi>Ga/mi>mprescripts>/mprescripts>none>/none>mn>76/mn>/mmultiscripts>/math>

A. Chester, B. A. Brown, S. P. Burcher, M. P. Carpenter, J. J. Carroll, C. J. Chiara, P. A. Copp, B. P. Crider, J. T. Harke, D. E. M. Hoff, K. Kolos, S. N. Liddick, B. Longfellow, M. J. Mogannam, T. H. Ogunbeku, C. J. Prokop, D. Rhodes, A. L. Richard, O. A. Shehu, A. S. Tamashiro, R. Unz, and Y. Xiao

Phys. Rev. C **105**, 024319 — Published 17 February 2022

DOI: 10.1103/PhysRevC.105.024319

Half-life measurement of the 199-keV isomeric state in ^{76}Ga

A. Chester,[1,*] B. A. Brown,[1,2] S. P. Burcher,[3] M. P. Carpenter,[4] J. J. Carroll,[5] C. J. Chiara,[5] P. A. Copp,[4] B. P. Crider,[6] J. T. Harke,[3] D. E. M. Hoff,[3] K. Kolos,[3] S. N. Liddick,[1,7] B. Longfellow,[1,2,†] M. J. Mogannam,[1,7] T. H. Ogunbeku,[6] C. J. Prokop,[8] D. Rhodes,[1,2] A. L. Richard,[1,†] O. A. Shehu,[6,‡] A. S. Tamashiro,[9] R. Unz,[6] and Y. Xiao[1,6,§]

[1]*National Superconducting Cyclotron Laboratory, Michigan State University, East Lansing, Michigan 48824*

[2]*Department of Physics and Astronomy, Michigan State University, East Lansing, Michigan 48824*

[3]*Lawrence Livermore National Laboratory, Livermore, California 94550*

[4]*Physics Division, Argonne National Laboratory, Lemont, Illinois 60439*

[5]*DEVCOM/Army Research Laboratory, Adelphi, Maryland 20783*

[6]*Department of Physics and Astronomy, Mississippi State University, Mississippi State, Mississippi 39762*

[7]*Department of Chemistry, Michigan State University, East Lansing, Michigan 48824*

[8]*Los Alamos National Laboratory, Los Alamos, New Mexico 87545*

[9]*School of Nuclear Science and Engineering, Oregon State University, Corvallis, Oregon 97331*

(Dated: January 28, 2022)

Abstract

Background: Isomeric states in atomic nuclei are a sensitive probe of their underlying microscopic structure and can be used to study the evolution of shell structure far from stability. Recent studies have identified and provided detailed spectroscopy of isomers in neutron-rich nuclei with $Z = 28$ - 50. Isomeric states in the odd-odd gallium isotopes have been reported for all gallium isotopes from $A = 72$ to $A = 80$ with the exception of ^{76}Ga.

Purpose: The purpose of this experiment was to observe short-lived isomeric states in the vicinity of ^{78}Ni.

Methods: In-beam fragmentation of a ^{86}Kr primary beam at the National Superconducting Cyclotron Laboratory produced radioactive ions which were delivered to and deposited in a $CeBr_3$ scintillator coupled to a position-sensitive photomultiplier tube. Beta-delayed γ rays were measured by ancillary HPGe clover and $LaBr_3$ detectors which surrounded the implantation detector.

Results: The previously observed $J^\pi = 1^+$, 199-keV level in ^{76}Ga, populated following the β decay of ^{76}Zn, was identified as isomeric with a half-life of $34(1)_{\text{stat.}}(8)_{\text{sys.}}$ ns. Shell-model calculations suggest this state is formed by the coupling of protons in negative-parity configurations to $1/2^-$ neutron configurations. Transition strengths assuming a ground-state spin of $J = 2$ and $J = 3$ were determined from the experimental data.

I. INTRODUCTION

The odd-odd, mid-shell gallium isotopes between $A = 72$ and $A = 80$ undergo an inversion of ground-state spin due to the lowering of the $\pi 0f_{5/2}$ orbital below the $\pi 1p_{3/2}$ orbital as the $\nu 0g_{9/2}$ orbital is filled [1, 2]. A change in ground-state spin/parity from $J^\pi = (3^-)$ in ^{74}Ga to $J^\pi = 2^-$ in ^{76}Ga occurs as the leading proton configuration in the ground state switches from $0f^1_{5/2}1p^2_{3/2}$ to $0f^3_{5/2}$. Additionally, a number of isomeric excited states have been identified in $^{72-80}$Ga [3–10]. Measuring the properties of these isomeric states can clarify the mechanisms driving shell evolution approaching the $N = 50$ shell gap as they

* Corresponding author: chester@frib.msu.edu

† Present address: Lawrence Livermore National Laboratory, Livermore, California 94550

‡ Present address: Department of Physics, University of Rhode Island, Kingston, Rhode Island, 02881

§ Present address: Department of Chemistry, University of Kentucky, Lexington Kentucky 40506

are sensitive to the underlying microscopic structure of the nuclei in which they appear. Further studies on the evolution of shell structure approaching doubly magic ^{78}Ni may also shed light on the predicted fifth island of inversion located past ^{78}Ni [11].

Negative-parity $J = 2$ and $J = 3$ isomeric states with energies less than 60 keV appear in ^{72}Ga [3, 4], ^{74}Ga [5, 6], and ^{80}Ga [8–10], with half-lives ranging from 31(5) ns to 1.3(2) s. In both ^{72,80}Ga, neutrons coupled to protons in the $0f_{5/2}$ orbit play a role in the appearance of these isomeric states [3, 8, 10]. Positive-parity $J = 0$ and $J = 1$ isomeric states formed by coupling $0f_{5/2}$ and $1p_{3/2}$ protons to $1p_{1/2}$ or $0f_{5/2}$ neutron hole configurations have been identified in the same nuclei, with half-lives ranging from 0.59(3) ns to 9.5(10) s. The excitation energies of the positive-parity isomers are higher on average than their negative-parity counterparts: 119 and 161 keV in the case of ^{72}Ga, 60 keV in ^{74}Ga, and 708 keV in ^{80}Ga. An isomeric state in ^{78}Ga at 560 keV has been identified with a 500 ns upper limit on the half-life though information regarding the spin and parity of the isomer are not known [7]. A candidate isomeric state with a half-life of 110(3) ns and energy of either 499 or 499+x keV was observed in Ref. [12].

Notably absent are data on isomeric states in ^{76}Ga. A detailed level scheme of ^{76}Ga following the β decay of the ^{76}Zn parent has been previously measured but no isomeric states were reported [13]. The present work has identified the $J^\pi = 1^+$, 199-keV state from Ref. [13] as isomeric with a half-life of $34(1)_{\text{stat.}}(8)_{\text{sys.}}$ ns determined by a combination of digital signal processing techniques and fast timing. Shell-model calculations, discussed in further detail in Sec. IV, suggest that the 1^+ isomeric state is highly mixed and arises due to the coupling of negative-parity proton and $1/2^-$ neutron configurations.

II. EXPERIMENTAL DETAILS

The experimental setup has been described in a previous publication, see Ref. [14], and only the salient details are repeated here. Radioactive ions were produced by in-beam fragmentation of a 140-MeV/nucleon beam of ^{86}Kr on a 320-mg/cm^2 ^{9}Be target at the National Superconducting Cyclotron Laboratory (NSCL). Ions of interest were separated following the fragmentation reaction using the A1900 fragment separator [15] at a momentum acceptance of 4.6%. The separated radioactive ion beam was delivered to an experimental end station consisting of three silicon detectors for particle identification and light-ion rejection

located approximately one meter upstream of a $CeBr_3$ scintillator detector. The beam was implanted into the $CeBr_3$ scintillator which was optically coupled to a position-sensitive photomultiplier tube (PSPMT) consisting of a single dynode and a 16×16 pixellated anode grid consisting of 256 3 mm $\times$ 3 mm anode pixels [16].

Beam particles were identified event-by-event based on their energy deposition in one of the silicon detectors and their time-of-flight between a position-sensitive scintillator located at the dispersive plane of the A1900 and one of the silicon detectors upstream of the implantation detector. Only a single $A = 76$ species, ^{76}Cu, was identified from the implanted ions. The ^{76}Ga nuclei of interest are the granddaughters of ^{76}Cu and were produced following the β decay of its daughter ^{76}Zn. A particle-identification plot highlighting the implanted ^{76}Cu ions is provided in Fig. 1. A combination of spatial and temporal information recorded by the PSPMT was used to correlate β-decay events with the implanted ions.

Two ancillary detector systems were present to record β-delayed γ rays: 16 HPGe clover detectors for high-resolution spectroscopy were arranged in a rhombicuboctahedron around the implantation detector and 15 $LaBr_3$ detectors [17], in triangular groups of three, were placed between the clover detectors. In order to minimize absorption of γ rays in the beamline and photomultiplier tube components downstream of the $CeBr_3$ scintillator, 12 $LaBr_3$ detectors were placed upstream of the center of the array while the remaining three detectors were installed in a downstream opening. The NSCL Digital Data Acquisition System (DDAS) [18] was used to process signals from all of the detector systems. For optimal timing performance the PSPMT dynode and $LaBr_3$ detectors were instrumented using a single 500 MSPS, 14-bit ADC. DDAS was used to record pulse shape traces for the PSPMT dynode signal. The dynode traces had a total length of 400 ns and a 120-ns delay.

Recorded dynode traces were analyzed to identify isomeric transitions populated by β decay. Such traces contain two pulses that are separated in time. An example of a dynode trace exhibiting this characteristic feature is shown in Fig. 2. A logistic function multiplied by an exponential decay was used to model the detector response. Traces recorded by DDAS were fit with both one and two model response functions plus a constant background term and the best-fit parameters were determined using χ^2 minimization. Double-pulse events were identified by comparing the χ^2 values of the two fits. An order-of-magnitude reduction in the χ^2 for the double-pulse fit, $\chi^2_{\text{single}}/\chi^2_{\text{double}} > 10$, was required to classify a recorded trace as a double pulse. An example best-fit two-pulse model is superimposed on the recorded

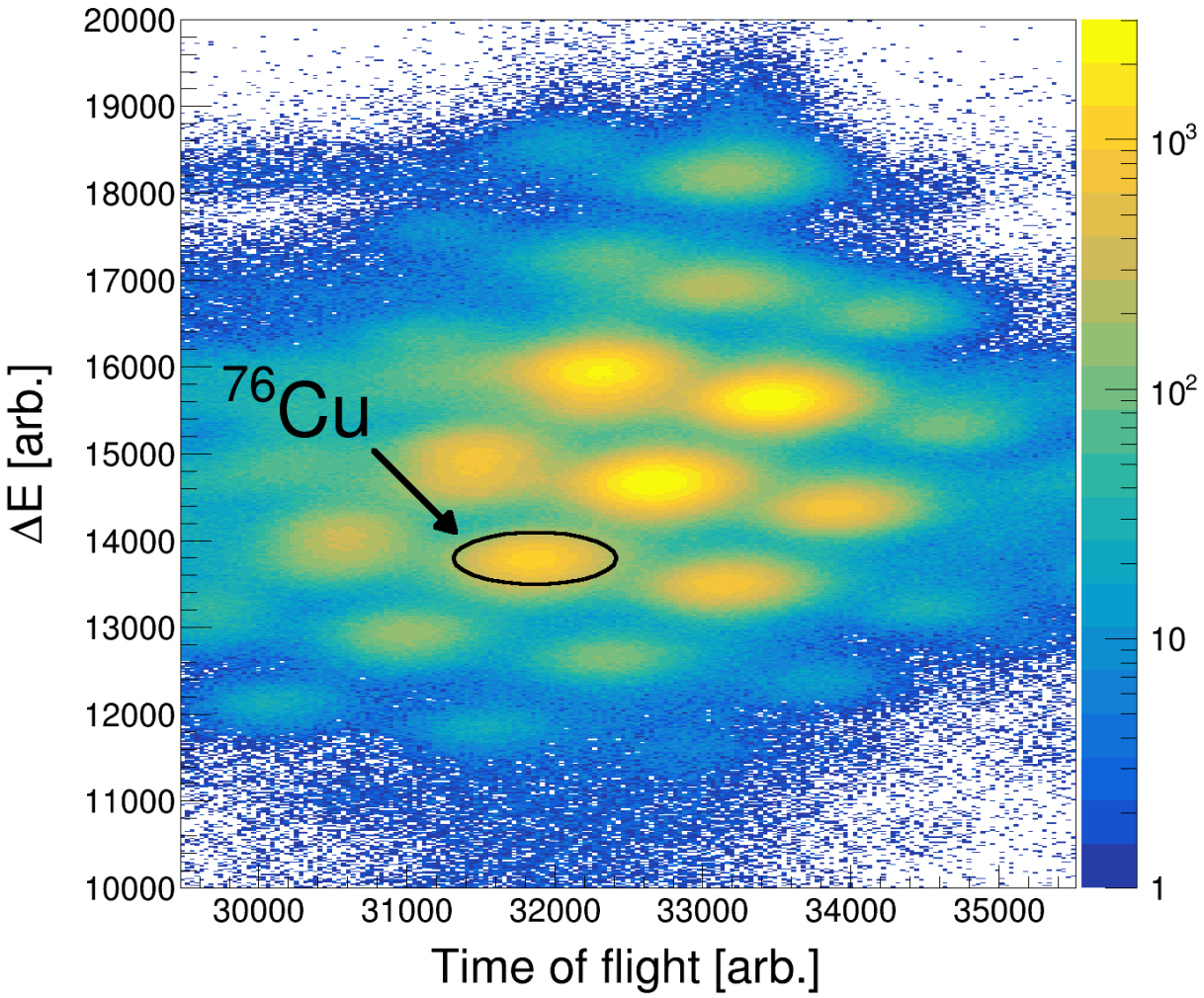

FIG. 1. (Color online). Particle-identification plot of ions implanted in the $CeBr_3$ detector. The ^{76}Cu ions are circled. The ^{76}Ga isotopes of interest in this work are the granddaughters of ^{76}Cu and were produced following the β decay of ^{76}Cu and its daughter nucleus ^{76}Zn. This figure is reproduced from Ref. [14].

trace shown in Fig. 2. The energies of the two pulses E_1 and E_2 and time difference between the first and second pulse $\Delta t = t_2 - t_1$ were saved for further analysis. To facilitate selective identification of double-pulse events, a minimum time difference between the first and second pulse of 20 ns was required.

Excited states in ^{76}Ga were populated following the β decay of ^{76}Zn, the daughter nucleus of the implanted ^{76}Cu ions. Beta-delayed γ rays recorded in the clover and $LaBr_3$ detectors up to 18 s following the detection of a ^{76}Cu ion were correlated with that implanted ion.

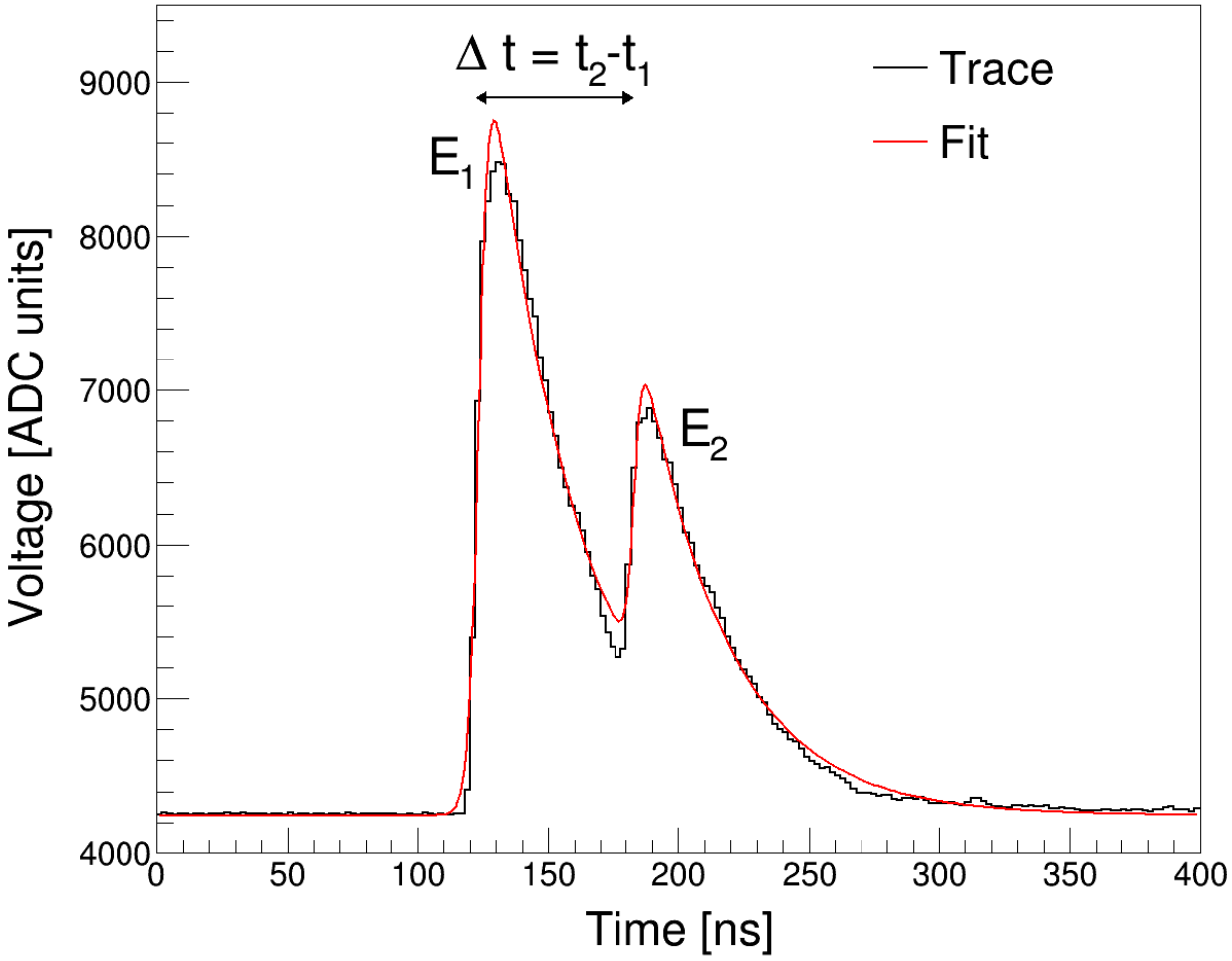

FIG. 2. (Color online). A recorded double-pulse signal from the PSPMT dynode characteristic of an isomeric transition populated following β decay. The response function described in Sec. II which has been fit to the recorded trace is shown in red. Pulse energies E_1 and E_2 and the time difference $\Delta t = t_2 - t_1$ between the two signals were determined from the best-fit parameters and used for further analysis.

The long correlation window of 18 s was chosen to account for the half-lives of both ^{76}Cu [$T_{1/2}$ = 0.641(6) s] and ^{76}Zn [$T_{1/2}$ = 5.7(3) s] [19]. Two previously observed γ rays from ^{76}Ga, with energies of 199 and 366 keV [13], are present in the background-subtracted γ-ray spectrum correlated with ^{76}Cu implants along with transitions belonging to the ^{76}Zn daughter nucleus [20] as shown in Fig. 3.

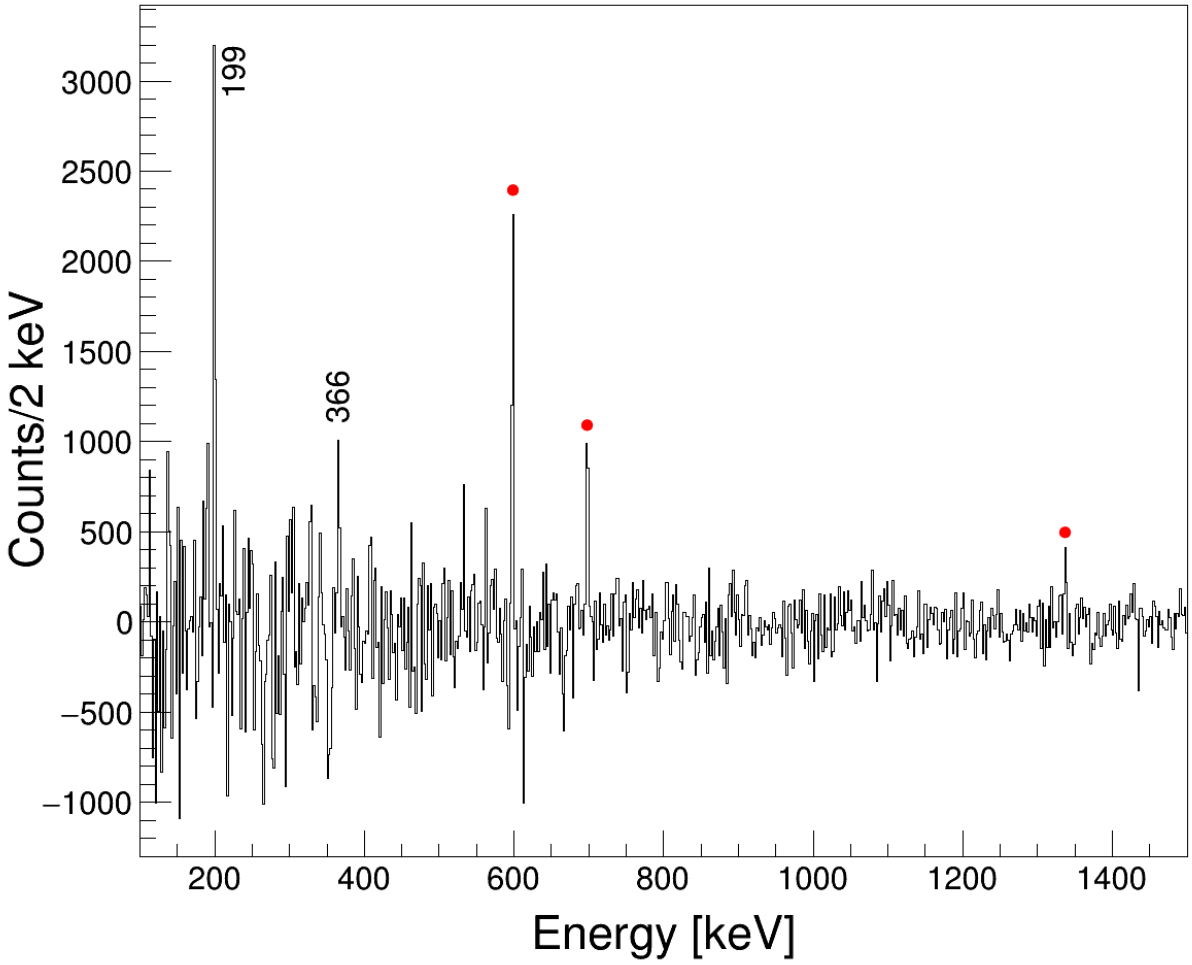

FIG. 3. (Color online). Background-subtracted, β-delayed γ rays detected within 18 s of a ^{76}Cu implant. Two γ-ray transitions previously observed in ^{76}Ga from Ref. [13] are labeled. The red circles denote known γ rays from the ^{76}Zn daughter [20], which are also observed within the correlation window.

III. ANALYSIS

Isomeric transitions following β decay have a unique signature in the energy spectrum of double-pulse events. The first pulse and associated energy E_1 of the double-pulse signature is attributed to the β-decay electron and will have a broad distribution of energies. The distribution in the second-pulse energy, E_2, arising from the isomeric transition will be narrower, though it may be broadened as well if the isomeric transition lies above a γ-ray cascade [14]. A plot of E_2 versus E_1 for double-pulse events is shown in Fig. 4. Also shown

on Fig. 4 is the gating region for the 199-keV ^{76}Ga isomeric transition of interest. The gap in the E_1 energy distribution in Fig. 4 is caused by an artifact of the trace fitting algorithm when the dynode trace has overflowed the ADC.

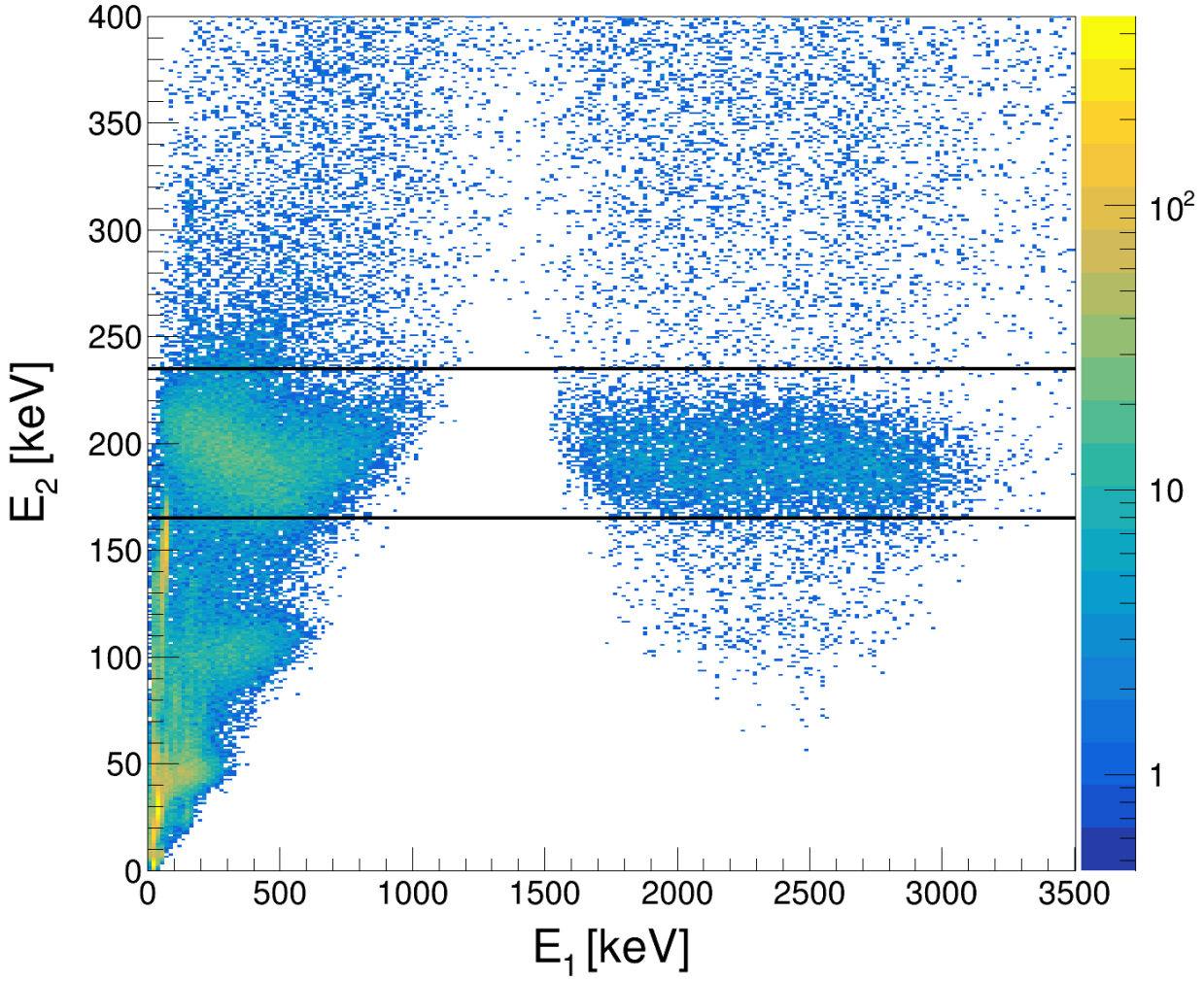

FIG. 4. (Color online). The double-pulse energy spectrum for pulses separated by more than 20 ns in the dynode trace. The energy of the second pulse, E_2, is plotted against the energy of the first pulse, E_1. A gating region around the 199-keV transition of interest is given by the horizontal black lines. For more details, refer to Sec. III.

Analysis of γ-ray transitions in coincidence with the isomeric transition recorded in the double-pulse energy spectrum was used to identify the isomer as the 199-keV state in ^{76}Ga. The coincident γ-ray energy spectrum measured in the clover detectors is shown in Fig. 5. All of the labeled transitions in Fig. 5 are known to be in coincidence with the 199-keV

transition in ^{76}Ga [13]. Only the 366-keV transition and unresolved 749-, 755-keV doublet are visible in the coincident $LaBr_3$ spectrum shown in Fig. 6 due to the lower γ-ray detection efficiency. A level scheme of the observed transitions based on Ref. [13] is given in Fig. 7. The previously observed 82-keV transition which connects the 281- and 199-keV states was not seen in this work due to its low relative intensity and absorption in the $CeBr_3$ detector; the same is true for the 95-keV transition connecting the 370- and 275-keV states. Coincidences through both the 82- and 95-keV transitions were observed as shown in Figs. 5-7.

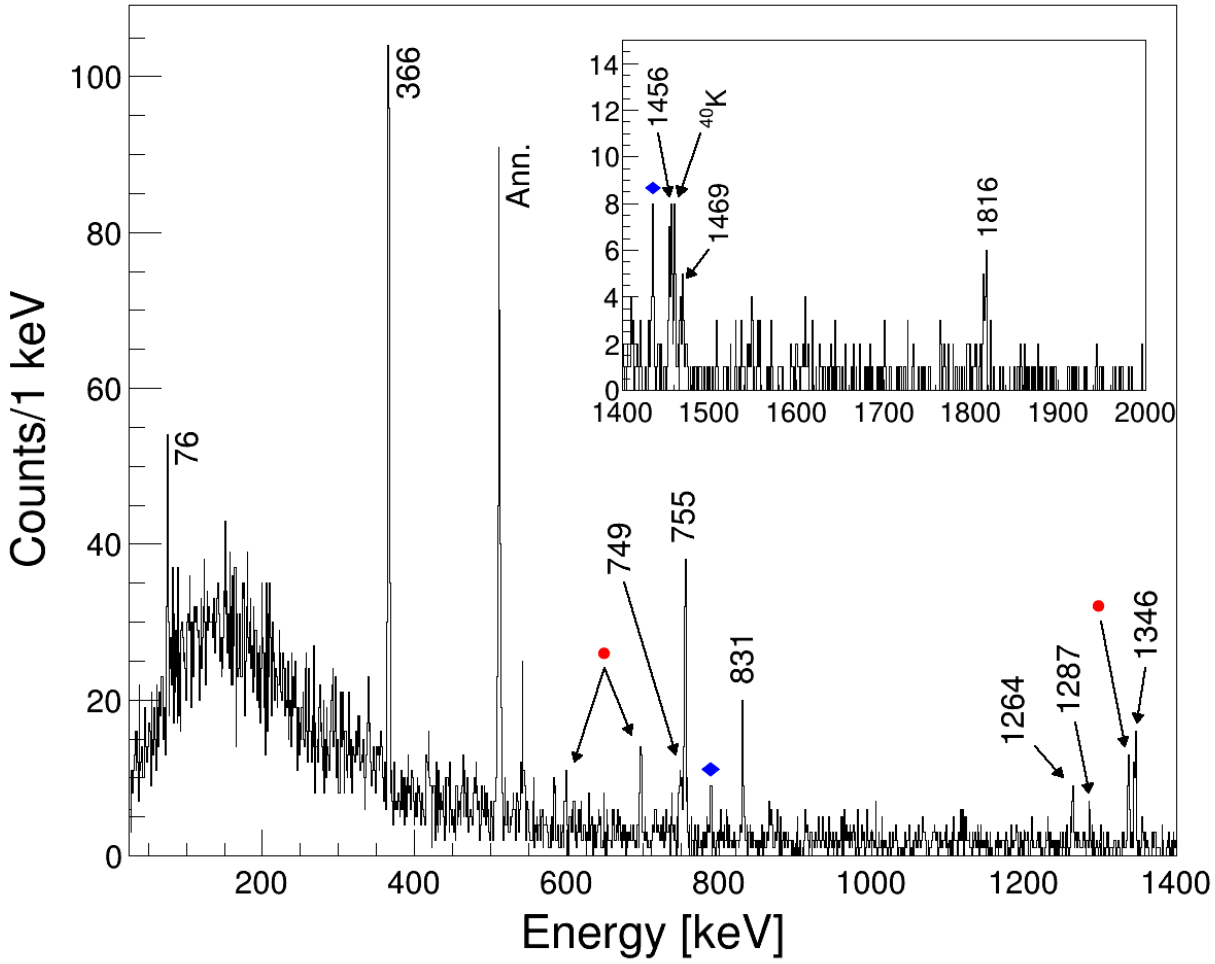

FIG. 5. (Color online). Gamma rays observed in coincidence with the double-pulse gate shown in Fig. 4 measured by the clover array. The peaks labeled by their energies are γ rays known to be in coincidence with the 199-keV transition in ^{76}Ga [13]. Background γ rays from ^{76}Zn (red circles), $LaBr_3$ internal activity (blue diamonds), e^+e^- annihilation, and ^{40}K are also shown. Note that the 199-keV γ ray is absent in this spectrum.

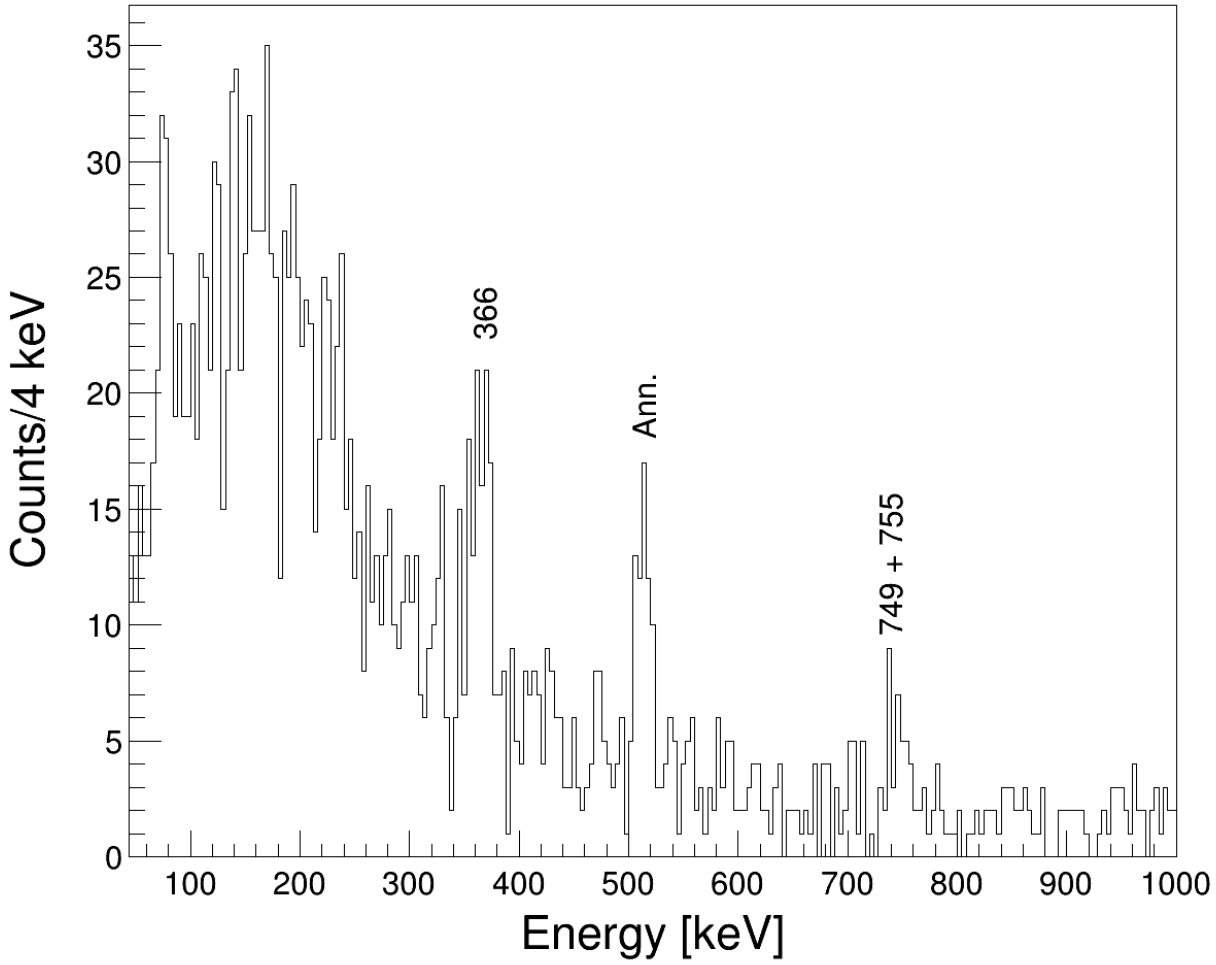

FIG. 6. Gamma rays coincident with the double-pulse gate shown in Fig. 4 measured by the $LaBr_3$ detectors. The peaks labeled by their energies are γ rays known to be in coincidence with the 199-keV transition in ^{76}Ga. The two peaks at 749 and 755 keV appear as one peak in this spectrum due to the detector energy resolution.

Efficiency-corrected γ-ray intensities of the observed transitions relative to the number of 199-keV isomeric state decays are presented in Table I. The relative intensity of the 76-keV transition is not reported here because the large interaction probability in the $CeBr_3$ crystal complicates the measurement of the clover efficiency using calibration sources. The relative intensity of the 366-keV transition, which is the most intense observed peak in both the clover and $LaBr_3$ spectra is in agreement with the expected value.

The half-life of the 199-keV state was determined using two independent methods. The first method utilized the dynode trace fit information to measure the distribution of time dif-

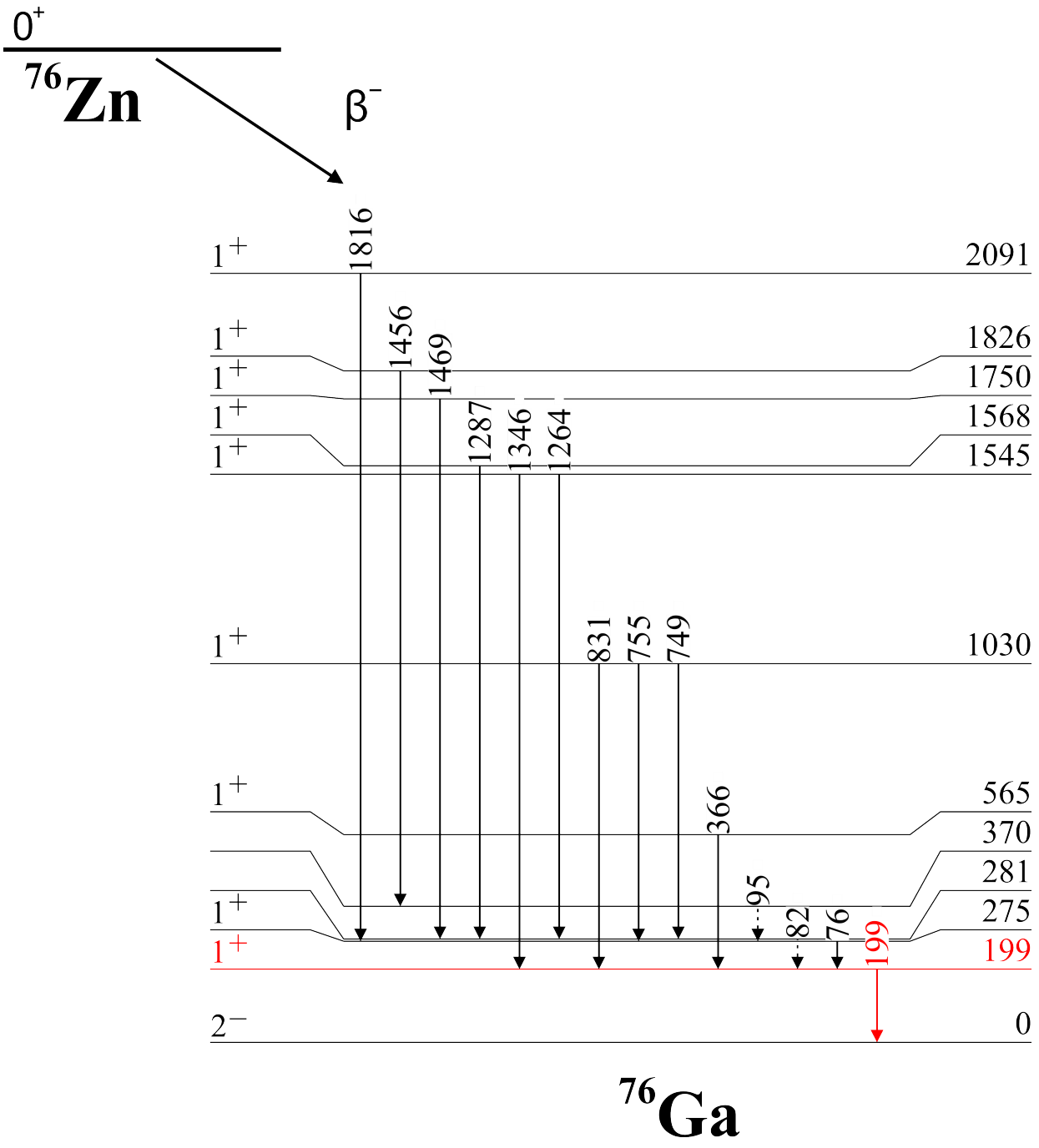

FIG. 7. (Color online). A level scheme showing the transitions observed in coincidence with the 199-keV isomeric transition in ^{76}Ga with energies given on the right in keV. The spin and parity assignments of the ground state and excited states are taken from Refs. [2] and [13] and are shown on the left side of the level. Unobserved transitions at 82 and 95 keV are given by dashed arrows. The 199-keV isomeric state and its depopulating transition identified in this work are shown in red.

TABLE I. Relative intensities of γ rays observed in the clover and $LaBr_3$ spectra shown in Figs. 5 and 6, respectively, normalized to the intensity of the 199-keV isomeric transition. The reported intensities, given in percent, have been corrected using the measured efficiency of the clover and $LaBr_3$ detectors. Expected relative intensities taken from Ref. [13] are shown in the third column. Statistical uncertainties at 1σ are shown in parentheses.

Energy [keV]	Clover	$LaBr_3$	Expected
366	8.8(12)	10(3)	9.7(4)
749	1.5(4)		3.7(4)
755	4.6(8)		5.3(3)
831	1.9(5)		2.2(2)
1264	0.9(3)		1.6(2)
1287	0.6(3)		0.73(5)
1346	2.6(6)		1.8(2)
1456	1.5(4)		1.1(2)
1469	0.9(3)		1.2(1)
1816	1.4(5)		0.88(5)

ferences between the first and second pulses recorded in double-pulse events. An exponential fit to the distribution of time differences, gated on the observed transitions in coincidence with the 199-keV transition, resulted in a measured half-life of 33.9(11) ns which is shown in Fig. 8. The second method used to determine the half-life leveraged the fast-timing characteristics of the $CeBr_3$ and $LaBr_3$ detectors. The timing response between the two detectors was calibrated using a combination of prompt γ rays emitted following β decay and a ^{60}Co source. A level lifetime of greater than approximately 1 ns will manifest as an exponential tail superimposed on the Gaussian prompt response peak. The time-difference spectrum for events where a 199-keV γ ray was detected in the $LaBr_3$ detectors and a β particle was detected in the $CeBr_3$ scintillator, again gated on transitions which feed the 199-keV level, is given in Fig. 9. A background spectrum, shown by the dashed line on Fig. 9, was constructed by averaging time profiles of energy regions located above and below the 199-keV transition. A best-fit half-life of 30(4) ns was determined by fitting an exponentially-modified Gaussian distribution (EMG) plus the background spectrum to the data. A systematic uncertainty

of 6 ns was obtained for each analysis method used to measure the half-life by varying the range over which the data was fit. The final reported half-life for the isomeric state is $34(1)_{\text{stat.}}(8)_{\text{sys.}}$ ns which was determined from the weighted average of these two methods with the systematic uncertainties added in quadrature.

IV. DISCUSSION

Calculations were carried out in the jj44 model space with the jun45, jj44b, and jj44c Hamiltonians described in detail in the Appendix of Ref. [21]. The levels for ^{76}Ga below 1 MeV are compared to experiment in Fig. 10. The blue lines are those with negative parity and the red lines are those with positive parity. The J value of the level is indicated by the length of the line. In this odd-odd nucleus there are about 35 states predicted below 1 MeV. Only a few of these have been observed experimentally, in particular, the 1^+ states suggested by the β decay of ^{76}Zn. While previous studies in ^{72,80}Ga attributed the $J = 1$ isomeric states to the coupling of $0f_{5/2}$ and $1p_{3/2}$ protons to $1p_{1/2}$ or $0f_{5/2}$ neutron hole configurations [3, 8, 10], the shell-model calculations performed here indicate the positive-parity states in ^{76}Ga are highly mixed and are constructed through the coupling of negative-parity proton and $1/2^-$ neutron configurations. The energies of the positive-parity states are correlated with the energy of the $1/2^-$ state in ^{73}Ni, calculated to be at (0.80, 0.70, 0.27) MeV for (jj44b, jj44c, jun45). The experimental energy of the $1/2^-$ state in ^{73}Ni is not known. The observed energy of the lowest 1^+ state in ^{76}Ga is (0.26, 0.29, 0.15) MeV lower than predicted by the three Hamiltonians. Thus, if all positive-parity states would be shifted down by that energy, the ground state could be $J^\pi = 2^+$. However, the 2^- state, lying at (0.072, 0.201, 0.071) MeV, has been firmly established as the ground state of ^{76}Ga in Ref. [2].

The 1^+ state at 199 keV decays to the 2^- ground state with a half-life of $34(1)_{\text{stat.}}(8)_{\text{sys.}}$ ns. Thus, the $B(E1)$ value is $1.60(5)_{\text{stat.}}(40)_{\text{sys.}} \times 10^{-6}$ $e^2\text{fm}^2$, which is in the range of observed $E1$ strengths for this mass region [22]. It should be noted that though $E1$ decay is forbidden in the jj44 model space, it does occur due to small admixtures from orbitals outside of the model space, namely those with a $0f_{7/2}$ proton hole or one neutron in the $1d_{5/2}$ or $2s_{1/2}$ orbitals. If the ground state would be assumed to have a positive parity, then the $B(M1)$ strength would be $1.50(5)_{\text{stat.}}(40)_{\text{sys.}} \times 10^{-4}$ μ_N^2, which is smaller than the

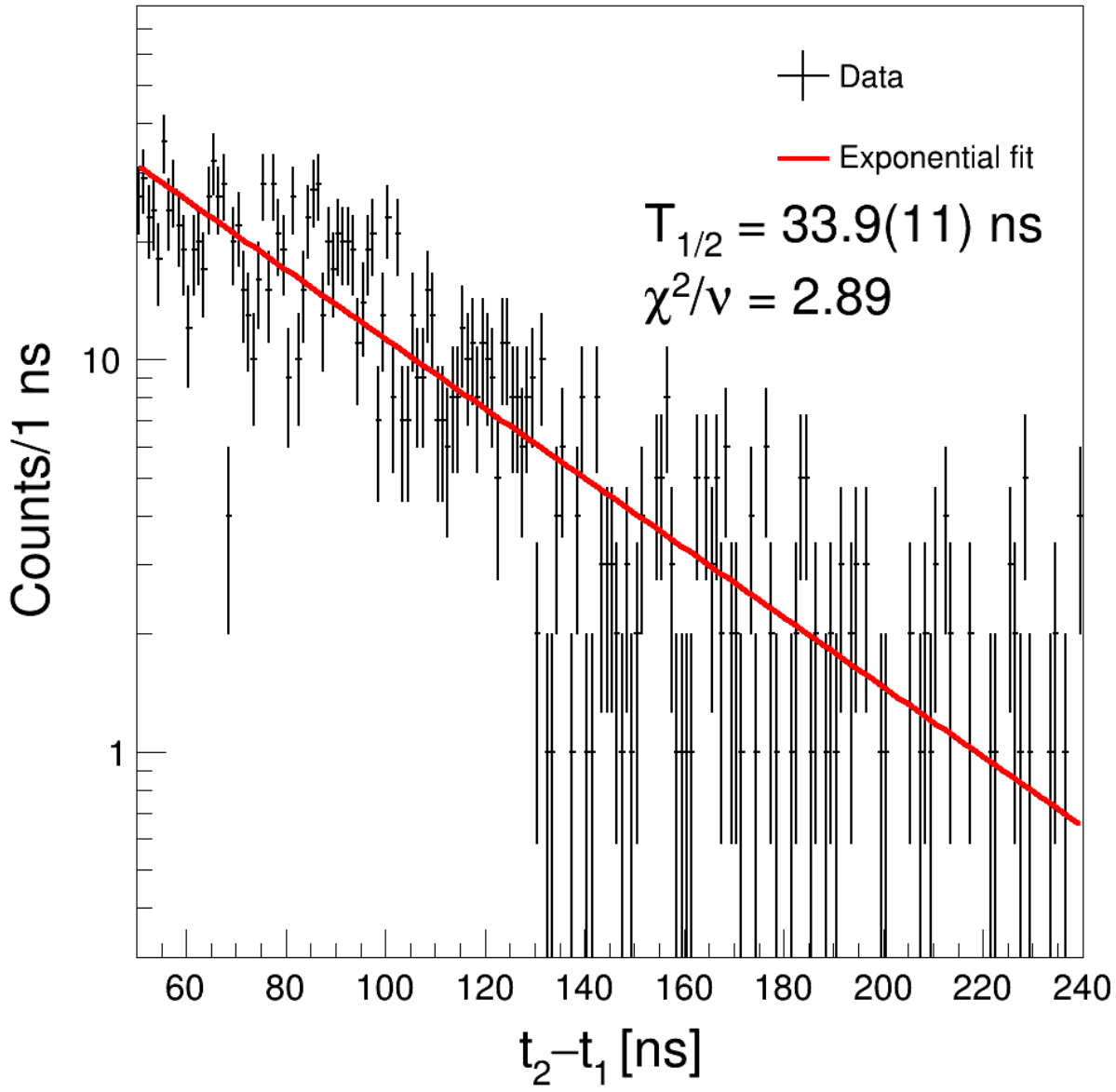

FIG. 8. (Color online). The distribution of time differences between the first (t_1) and second (t_2) pulses for double-pulse events contained in the gating region shown in Fig. 4, constructed from the fit parameters of the model detector response described in Sec. II (black). A gate on the observed γ rays in coincidence with the 199-keV isomer was applied to the time-difference distribution. The time difference was fit with an exponential function (red) resulting in a measured half life of 33.9(11) ns with the statistical uncertainty at 1σ given in parentheses.

calculated value of 24×10^{-4} μ_N^2. However, this could be consistent with theory given the large theoretical uncertainties for small $B(M1)$ values. The shell-model calculations indicate

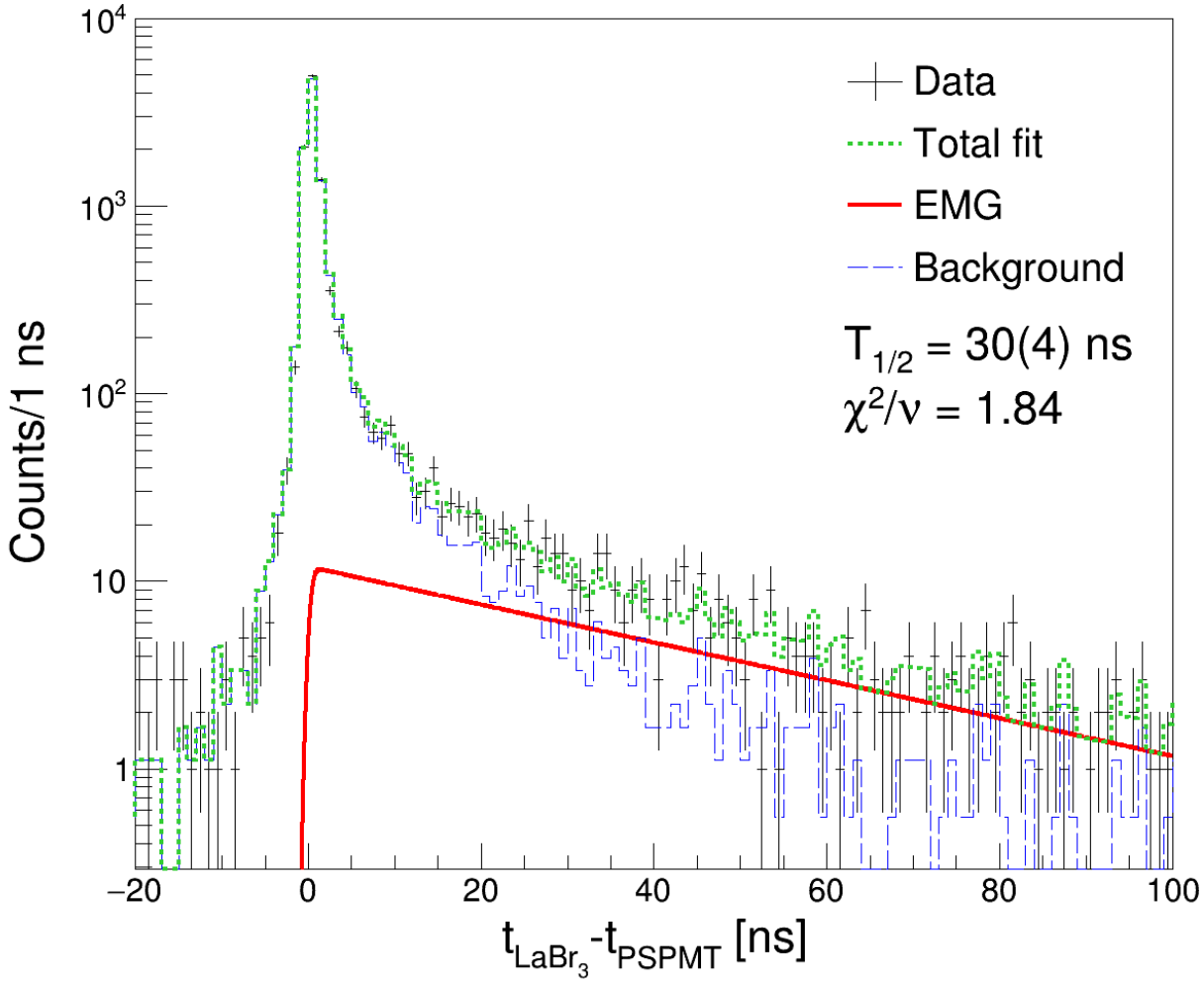

FIG. 9. (Color online). Time-difference distribution for events where a 199-keV γ ray was detected in a $LaBr_3$ detector and a β particle was detected in the $CeBr_3$ scintillator (black). The distribution was gated on the transitions which feed the 199-keV level. A background (blue dashed line) was determined by averaging the time-difference distributions of energy regions located above and below the 199-keV transition. The total fit to the data (green dotted line) incorporates both the background and the EMG (red), which is sensitive to the half-life. The best-fit half-life determined using this method is 30(4) ns with the statistical uncertainty at 1σ given in parentheses.

that a $J^\pi = 3^-$ ground state is also possible. The $B(M2)$ value of this transition would be $4900(160)_{\text{stat.}}(1200)_{\text{sys.}}$ $\mu_N^2\text{fm}^2$, which is large compared to both the calculated value of 0.62 $\mu_N^2\text{fm}^2$ as well as the recommended upper limit of 30 $\mu_N^2\text{fm}^2$ based on a survey of transition strength data for nuclei with A = 45-150 [23]. Based on the possible transition strengths, the present result is in agreement with the previous assignment of a 2^- ground-

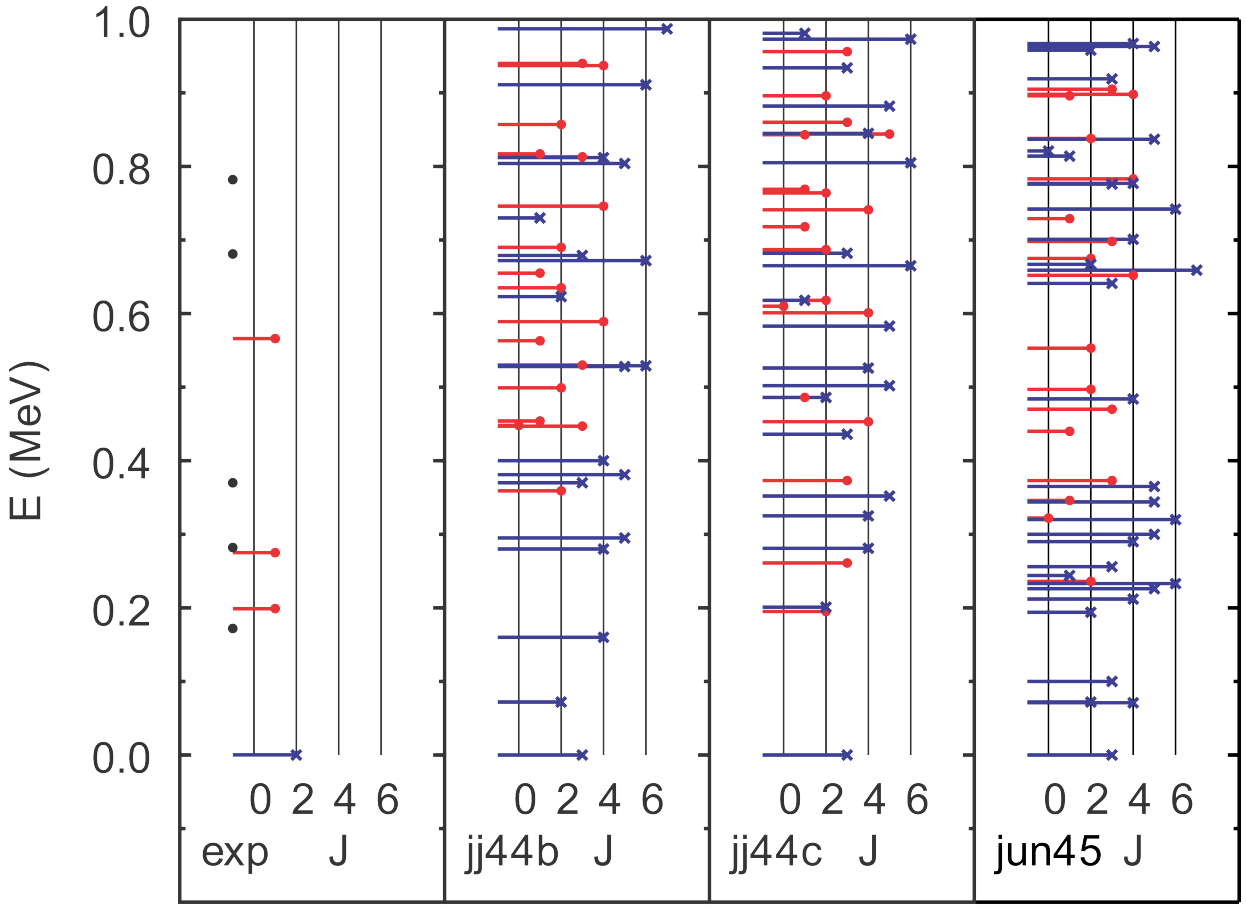

FIG. 10. (Color online). Comparison of experimental levels from Ref. [13] and calculated levels using the jj44 interaction with $J \leq 6$ and energies up to 1 MeV. Negative-parity levels are shown in blue and positive-parity levels in red. The spin of the level is given by the horizontal length of the bar. Experimentally observed levels with unknown spin and parity are denoted by the black dots. The observed energy of the lowest-lying, 199-keV 1^+ state in ^{76}Ga is (0.26, 0.29, 0.15) MeV lower than predicted by the three Hamiltonians.

state spin-parity for ^{76}Ga [2]. A comparison of the transition rates to possible ground-state spin/parity assignments from shell-model calculations is not sensitive enough to distinguish between positive- and negative-parity ground states, although it is sensitive to the spin. Known isomeric states in the odd-odd gallium isotopes from $A = 72$ to $A = 80$, including previously observed 1^+ isomeric states in ^{72,80}Ga and the 199-keV isomeric state in ^{76}Ga identified in this work, are summarized on Fig. 11.

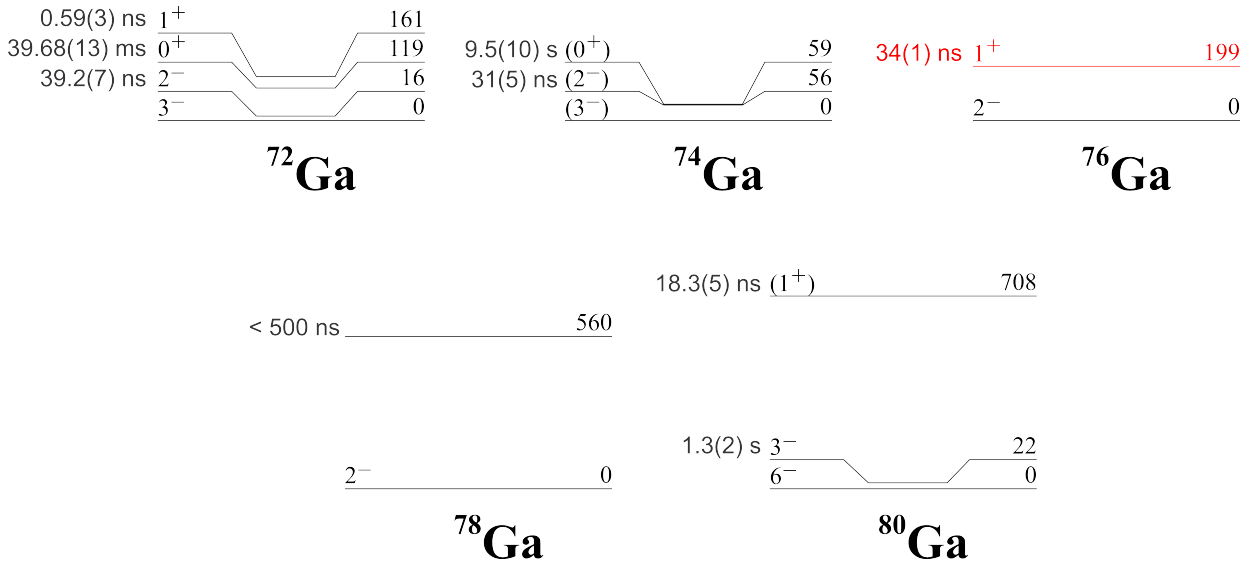

FIG. 11. (Color online) Systematics of known isomeric states in the odd-odd gallium isotopes from Refs. [3–10] with the present results for ^{76}Ga shown in red. Energies in keV are given on the right of the levels and their corresponding spin and parity assignments are shown on the left. The level half-life is shown next to the spin/parity with the statistical uncertainty at 1σ in parentheses. The isomeric state in ^{78}Ga is consistent with a 110(3) ns isomer observed in Ref. [12] if the state is located above 499 keV.

V. CONCLUSIONS

The 199-keV state in ^{76}Ga, populated following the β decay of ^{76}Zn, has been identified as isomeric with a half-life of $34(1)_{\text{stat.}}(8)_{\text{sys.}}$ ns. Shell-model calculations indicate this state has a highly mixed character, formed from the coupling of negative-parity proton configurations with $1/2^-$ neutron configurations. Transition strengths for an $E1$ or $M1$ transition to states with a spin $J = 2$ give values that are consistent with previous surveys of data, while the transition strength to the theoretically observed spin $J = 3$ level results in an unrealistic transition strength. While the parity cannot be firmly established from the transition strengths, we can confirm that the ground state spin is $J = 2$, in agreement with the established $J^\pi = 2^-$ from Ref. [2]. The observation and characterization of the 199-keV isomeric state highlights the role that negative-parity proton and neutron orbitals have on the evolution of nuclear shell structure in the neutron-rich gallium isotopes which lie near the doubly-magic nucleus ^{78}Ni.

ACKNOWLEDGMENTS

This work was supported by the US Department of Energy (DOE) National Nuclear Security Administration Grant No. DOE-DE-NA0003906, the Nuclear Science and Security Consortium under Award No. DE-NA0003180, the DOE Office of Nuclear Physics under Grant No. DE-SC0020451, and Contract No. DE-AC02-06CH11357 (Argonne National Laboratory). Additional support was provided under the auspices of the DOE by the Lawrence Livermore National Laboratory (LLNL) under Contract No. DE-AC52-07NA27344 and the Laboratory Directed Research and Development (LDRD) program at LLNL under project 21-FS-011. Further support was provided by the National Science Foundation (NSF) Grant No. PHY-1848177 (CAREER) (Mississippi State University) and NSF Grant No. PHY-1811855. This work was supported in part through computational resources and services provided by the Institute for Cyber-Enabled Research at Michigan State University.

[1] B. Cheal, E. Mané, J. Billowes, M. L. Bissell, K. Blaum, B. A. Brown, F. C. Charlwood, K. T. Flanagan, D. H. Forest, C. Geppert, M. Honma, A. Jokinen, M. Kowalska, A. Krieger, J. Krämer, I. D. Moore, R. Neugart, G. Neyens, W. Nörtershäuser, M. Schug, H. H. Stroke, P. Vingerhoets, D. T. Yordanov, and M. Žáková, Phys. Rev. Lett. **104**, 252502 (2010).

[2] E. Mané, B. Cheal, J. Billowes, M. L. Bissell, K. Blaum, F. C. Charlwood, K. T. Flanagan, D. H. Forest, C. Geppert, M. Kowalska, A. Krieger, J. Krämer, I. D. Moore, R. Neugart, G. Neyens, W. Nörtershäuser, M. M. Rajabali, R. Sánchez, M. Schug, H. H. Stroke, P. Vingerhoets, D. T. Yordanov, and M. Žáková, Phys. Rev. C **84**, 024303 (2011).

[3] H. Kugler, Nuclear Physics A **137**, 281 (1969).

[4] O. Brandstdter, F. Girsig, F. Grass, and R. Klenk, Nuclear Instruments and Methods **104**, 45 (1972).

[5] J. van Klinken and L. M. Taff, Phys. Rev. C **9**, 2252 (1974).

[6] L. Taff and J. van Klinken, Nuclear Instruments and Methods **151**, 189 (1978).

[7] C. M. Folden, A. S. Nettleton, A. M. Amthor, T. N. Ginter, M. Hausmann, T. Kubo, W. Loveland, S. L. Manikonda, D. J. Morrissey, T. Nakao, M. Portillo, B. M. Sherrill, G. A. Souliotis, B. F. Strong, H. Takeda, and O. B. Tarasov, Phys. Rev. C **79**, 064318 (2009).

[8] B. Cheal, J. Billowes, M. L. Bissell, K. Blaum, F. C. Charlwood, K. T. Flanagan, D. H. Forest, S. Fritzsche, C. Geppert, A. Jokinen, M. Kowalska, A. Krieger, J. Krämer, E. Mané, I. D. Moore, R. Neugart, G. Neyens, W. Nörtershäuser, M. M. Rajabali, M. Schug, H. H. Stroke, P. Vingerhoets, D. T. Yordanov, and M. Žáková, Phys. Rev. C **82**, 051302(R) (2010).

[9] D. Verney, B. Tastet, K. Kolos, F. Le Blanc, F. Ibrahim, M. Cheikh Mhamed, E. Cottereau, P. V. Cuong, F. Didierjean, G. Duchêne, S. Essabaa, M. Ferraton, S. Franchoo, L. H. Khiem, C. Lau, J.-F. Le Du, I. Matea, B. Mouginot, M. Niikura, B. Roussière, I. Stefan, D. Testov, and J.-C. Thomas, Phys. Rev. C **87**, 054307 (2013).

[10] R. Lică, N. Mărginean, D. G. Ghiţă, H. Mach, L. M. Fraile, G. S. Simpson, A. Aprahamian, C. Bernards, J. A. Briz, B. Bucher, C. J. Chiara, Z. Dlouhý, I. Gheorghe, P. Hoff, J. Jolie, U. Köster, W. Kurcewicz, R. Mărginean, B. Olaizola, V. Paziy, J. M. Régis, M. Rudigier, T. Sava, M. Stănoiu, L. Stroe, and W. B. Walters, Phys. Rev. C **90**, 014320 (2014).

[11] F. Nowacki, A. Poves, E. Caurier, and B. Bounthong, Phys. Rev. Lett. **117**, 272501 (2016).

[12] J. M. Daugas, T. Faul, H. Grawe, M. Pfützner, R. Grzywacz, M. Lewitowicz, N. L. Achouri, J. C. Angélique, D. Baiborodin, R. Bentida, R. Béraud, C. Borcea, C. R. Bingham, W. N. Catford, A. Emsallem, G. de France, K. L. Grzywacz, R. C. Lemmon, M. J. Lopez Jimenez, F. de Oliveira Santos, P. H. Regan, K. Rykaczewski, J. E. Sauvestre, M. Sawicka, M. Stanoiu, K. Sieja, and F. Nowacki, Phys. Rev. C **81**, 034304 (2010).

[13] B. Ekström, B. Fogelberg, P. Hoff, E. Lund, and A. Sangariyavanish, Physica Scripta **34**, 614 (1986).

[14] A. Chester, B. A. Brown, S. P. Burcher, M. P. Carpenter, J. J. Carroll, C. J. Chiara, P. A. Copp, B. P. Crider, J. T. Harke, D. E. M. Hoff, K. Kolos, S. N. Liddick, B. Longfellow, M. J. Mogannam, T. H. Ogunbeku, C. J. Prokop, D. Rhodes, A. L. Richard, O. A. Shehu, A. S. Tamashiro, R. Unz, and Y. Xiao, Phys. Rev. C **104**, 054314 (2021).

[15] D. J. Morrissey, B. M. Sherrill, M. Steiner, A. Stolz, and I. Wiedenhoever, Nuclear Instruments and Methods in Physics Research Section B: Beam Interactions with Materials and Atoms **204**, 90 (2003).

[16] Data Sheet, *Flat panel type mutlianode PMT assembly H13700 series*, Hamamatsu Photonics KK, 314-5, Shimokanzo, Iwata City, Shizuoka Pref., 438-0193, Japan (2020), retrieved from: https://www.hamamatsu.com/resources/pdf/etd/H13700_TPMH1370E.pdf. Accessed 2 April 2021.

[17] B. Longfellow, P. C. Bender, J. Belarge, A. Gade, and D. Weisshaar, Nuclear Instruments and Methods in Physics Research Section A: Accelerators, Spectrometers, Detectors and Associated Equipment **916**, 141 (2019).

[18] C. J. Prokop, S. N. Liddick, B. L. Abromeit, A. T. Chemey, N. R. Larson, S. Suchyta, and J. R. Tompkins, Nuclear Instruments and Methods in Physics Research Section A: Accelerators, Spectrometers, Detectors and Associated Equipment **741**, 163 (2014).

[19] B. Singh, Nuclear Data Sheets **74**, 63 (1995).

[20] J. Van Roosbroeck, H. De Witte, M. Gorska, M. Huyse, K. Kruglov, D. Pauwels, J.-C. Thomas, K. Van de Vel, P. Van Duppen, S. Franchoo, J. Cederkall, V. N. Fedoseyev, H. Fynbo, U. Georg, O. Jonsson, U. Köster, L. Weissman, W. F. Mueller, V. I. Mishin, D. Fedorov, A. De Maesschalck, N. A. Smirnova, and K. Heyde, Phys. Rev. C **71**, 054307 (2005).

[21] S. Mukhopadhyay, B. P. Crider, B. A. Brown, S. F. Ashley, A. Chakraborty, A. Kumar, M. T. McEllistrem, E. E. Peters, F. M. Prados-Estévez, and S. W. Yates, Phys. Rev. C **95**, 014327 (2017).

[22] P. M. Endt, Atomic Data and Nuclear Data Tables **23**, 547 (1979).

[23] Nuclear Data Sheets **111**, viii (2010).